Original Article

Intravital assessment of angioarchitecture in rat hepatocellular nodules using *in vivo* fluorescent microscopy

Yi Liu[1#], Tao Lu[1#], Congcong Wang[1], Hui Li[2], Ke Xu[1], Peiling Li[1]

[1]Department of Radiology, The First Clinical Hospital of China Medical University, Shenyang 110001, China; [2]Department of Radiology, Shengjing Hospital of China Medical University, Shenyang 110004, China

[#]These authors contributed equally to this work.

Correspondence to: Peiling Li. Department of Radiology, The First Hospital of China Medical University, Shenyang 110001, China. Email: lipeilingcmu@163.com.

Background: To prospectively evaluate the stepwise changes that occur in intra-nodular microvessels and microcirculation during the carcinogenesis process of hepatocellular nodules by using *in vivo* fluorescent microscopy, and to compare these with pathological changes.

Methods: Forty-five 10-week-old male Wistar rats received drinking water containing N-nitrosomorpholine at 10 mg/100 mL for 18weeks to develop multiple hepatocellular carcinomas (HCC) and dysplastic nodules (DN) in the liver; meanwhile, the non-lesion liver tissues become fibrotic. The microvascular morphological change and hemodynamic change of two lesion areas (HCC or DN) and one non-lesion area in each rat were observed with *in vivo* fluorescent microscope. After *in vivo* microscopy, 90 nodules and 45 non-lesion liver tissues that were observed were removed for pathological study. The microvessel density (MVD), branch density (BD), and cell density (CD) of these lesions were compared with the Kruskal-Wallis test and Mann-Whitney test, with an overall statistical significance of 0.05.

Results: The intra-nodular microvessels appeared tortuous, with irregular branching and abrupt diameter changes to form irregular convoluted networks in the HCC. This was distinctly different from the appearance of DN and non-lesion liver parenchyma. The MVD and BD of HCC were less than that of the DN and non-lesion liver parenchyma ($P<0.01$), and the BD of DN was also less than that of the non-lesion liver parenchyma ($P<0.05$). However, the MVD of the DN was similar to that of the non-lesion liver parenchyma ($P>0.05$). The CD of HCC was more than that of the DN and non-lesion liver parenchyma ($P<0.05$), and the CD of DN was also more than that of the non-lesion liver parenchyma ($P<0.05$).

Conclusions: Concurrent with the carcinogenesis process of the hepatocellular nodule, both the intra-nodular microvascular morphology and hemodynamics were stepwise changed, and the number of the intravascular lumen of intranodular microvessels decreased due to the infiltration and compression of intra-nodular parenchymal cells.

Keywords: Hepatocellular carcinoma (HCC); hepatocellular dysplastic nodules; angioarchitecture; microvessel density (MVD); *in vivo* fluorescent microscopy

Submitted Feb 19, 2019. Accepted for publication Jun 13, 2019.
doi: 10.21037/qims.2019.06.11
View this article at: http://dx.doi.org/10.21037/qims.2019.06.11

Introduction

Hepatocellular carcinoma (HCC) is one of the most prevalent malignancies in the world (1-3). The majority of HCCs develops in cirrhotic livers and has been proven to develop by multi-step carcinogenesis from hepatocellular nodules. According to the classification system proposed by

© Quantitative Imaging in Medicine and Surgery. All rights reserved.

the International Working Party of the World Congress of Gastroenterology and the International Consensus Group for Hepatocellular Neoplasia (4,5), hepatocellular nodules can be divided into four main categories: large regenerative nodules (LRN), low-grade dysplastic nodules (DN), high-grade DN, and HCC. In daily clinical practice, the dual blood supply of the liver has aided diagnosis of these hepatocellular nodules with dynamic enhanced computed tomography (CT) and magnetic resonance (MR) images by providing an opportunity to image tumors during their preferential enhancement while the contrast medium is passing through the hepatic circulation system (6-8). However, the stepwise changes of CT and MR images of these hepatocellular nodules are heterogeneous, which make it very difficult to distinguish these lesions accurately; thus, it is very important to clearly understand the reason for these stepwise changes in imaging for clinical diagnosis. In the past two decades, some researchers have demonstrated the value of *in vivo* microscopy when it is applied to the study of intratumoral microvessel construction of hepatic lesions, showing that it allows for the intravital observation of microvessels without affecting natural hemodynamics (9-13). For this reason, this method should be mostly similar to contrast enhanced CT or MRI in clinical practice for the evaluation of liver parenchyma micro-circulation.

The present study was undertaken by using *in vivo* fluorescent microscopyto investigate the microcirculation and morphological changes of intranodular microvessels of rat hepatocellular nodules induced with 18 weeks of chemical intoxication.

Methods

This study was approved by the Ethics Review Board of the First Hospital of China Medical University and was performed in accordance with its guidelines. All experimental rats were obtained from the laboratory animal division of China Medical University.

Animal and tumor model

Forty-five 10-week-old male Wistar rats weighing 260 to 300 g received drinking water containing N-nitrosomorpholine at 10 mg/100 mL for 18 weeks. It is known that animals induced by this method develop multiple HCC and DN in the liver and that their non-lesion tissues become fibrotic (14,15).

In vivo study

In vivo microscopy was performed on exteriorized livers. In each rat, two lesion areas and one non-lesion area were observed. The morphologic and hemodynamic changes of intranodular microvessels were observed according to previously reported techniques. After injection of fluorescein sodium, the rats were transferred to the objective stage of an OlympusBH-2 microscope (Olympus, Optical Co., Tokyo, Japan) which was equipped with a mercury lamp (100 W) and a filter cube which selected blue light (450–490 nm) for epi-illumination interposed into the light path. Microscopic images were recorded in real-time with a digital video camera (DXC-108, Sony, Tokyo, Japan) and transferred to a DV video system (NV-DM1, Panasonic, Tokyo, Japan) for offline analysis (16). All rats underwent a single session of *in vivo* microscopy and then were sacrificed with an overdose of anesthetic. Microscopic images were recorded at a rate of 30 images per second with a digital video camera and were transferred to a computer for off-line analysis.

Image analysis

In vivo images of 90 nodules and 45 non-lesion areas were downloaded onto a computer equipped with software (Windows 2000) from videotapes by using a real-time digital video image capture card, and were analyzed with imaging software (Osiris; Digital Imaging Unit, University Hospital of Geneva, Geneva, Switzerland) and the software for quantitative analysis of angiogenesis network (Angiogenesis Image Analyzer; Kurabo Industries, Osaka, Japan). On *in vivo* images, the following data were collected: (I) intratumoral microvessel density (MVD), which was defined as a ratio of the areas between the intratumoral microvessels and tumor on the liver surface, and was calculated as the total area of observed intratumoral microvessels in one tumor divided by the extent of this tumor on the liver surface; and (II) intratumoral branch density (BD), which was evaluated to compare the morphological abnormality of intratumoral microvessels, and defined as the number of branches per square millimeter on the liver surface, and calculated as the number of branches in one tumor divided by the extent of this tumor on the liver surface.

Histological staining and analysis

The 90 nodules and 45 non-lesion liver tissues that were

© Quantitative Imaging in Medicine and Surgery. All rights reserved.

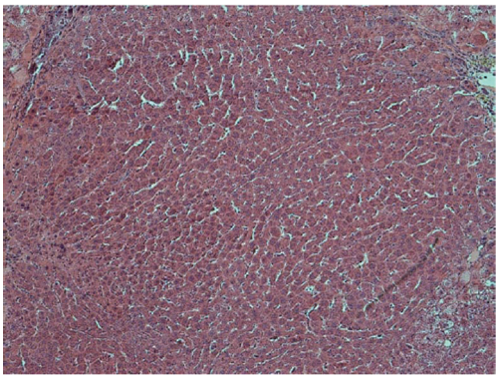

Figure 1 The histological image of regenerative nodules (HE staining, ×100). There was one terminal portal tract in the regenerative nodules, the hepatocyte plates were one-cell wide, the cells were histologically the same as those in adjacent parenchyma, and the sinusoids varied mildly in diameter.

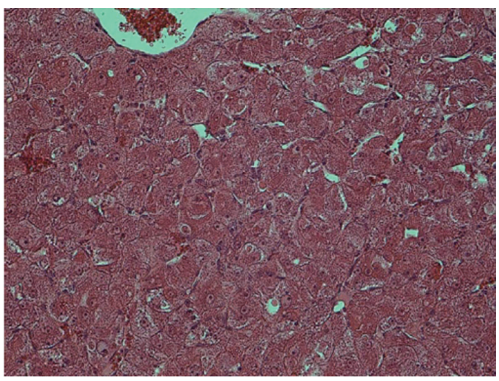

Figure 2 The histological image of low-grade dysplastic nodules (HE staining, ×200). The cells of low-grade dysplastic nodules were usually large and uniform, and differed from those of adjacent hepatocytes with minimal nucleus abnormalities and clone-like changes. The intra-nodular sinusoids were compressed by the large hepatocytes.

observed were removed after *in vivo* microscopy, the maximal diameter of each nodule was measured, and the specimen was then fixed in 10% formalin. They were embedded in paraffin, and 5 μm serial sections were cut for hematoxylin-eosin (HE) staining and histological analysis.

Histological examination was conducted by two hepatopathologists with at least 10 years of experience in liver pathology, and a consensus was achieved. According to the diagnostic criteria proposed by the International Working Party of the World Congress of Gastroenterology and the International Consensus Group for Hepatocellular

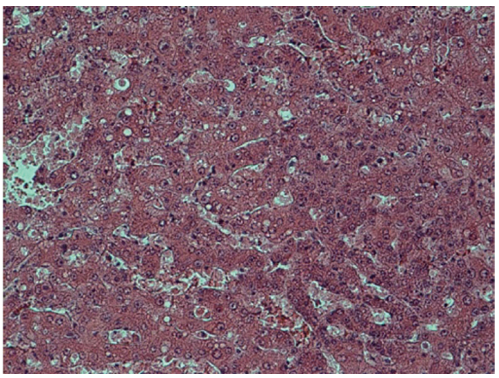

Figure 3 The histological image of high-grade dysplastic nodules (HE staining, ×200). There were usually multiple subpopulations of different cellular appearances in a high-grade dysplastic nodule; they differed from those of the adjacent hepatocytes with respect to cell and nuclear size, cytoplasmic staining, and degree of nucleus atypia. The intranodule cell plates were one or several cells wide, and partial intranodule sinusoids were compressed, while others were dilated.

Neoplasia (3,4), nodules were classified as (I) LRN, (II) low-grade DN, (III) high-grade DN, and (IV) HCC. LRN is a multiacinar nodule, and distinctly larger than most cirrhotic nodules found in the same liver, being generally ≥0.5 cm in greatest dimension (*Figure 1*). A DN is a nodular region of hepatocytes with dysplasia but without definite histologic criteria of malignancy; low-grade DN shows mild atypia and is differentiated from LRN by features of large liver cell change, minimal nuclear abnormalities, and clone-like changes that are not detected in LRN (*Figure 2*). High-grade DN shows at least moderate atypia, and it is characterized by (I) increased cellularity with a nucleus/cytoplasmic ratio 1.5 to 2 times more than that of adjacent cirrhotic nodules, (II) focal acinar arrangement, and (III) nodule-in-nodule lesions (*Figure 3*). Well-differentiated HCC shows increased cellularity and a nucleus/cytoplasmic ratio more than twice that of adjacent cirrhotic nodules and frequent acinar arrangement (*Figure 4*). In our study, the LRN was classified into background cirrhotic liver, and the DN category included both low- and high-grade DNs because they were occasionally confused on CT and MR images (1,2,6,7,17,18).

The HE-stained sections were used to determine cell density (CD). Five high power fields (×400) were selected within different parts of these nodules on each section. Cell nuclei were identified based on a blue color and a spherical shape. All nuclei within the fields were counted; the mean

© Quantitative Imaging in Medicine and Surgery. All rights reserved.

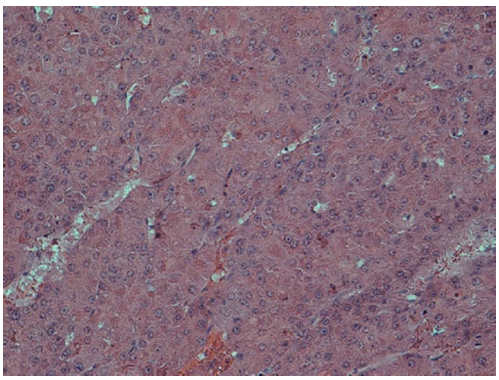

Figure 4 The histological image of hepatocellular carcinoma (HE staining, ×200). The cell size of the hepatocellular carcinomas decreased, the nuclear-cytoplasmic ratio was usually more than twice that of adjacent cirrhotic nodules, and the nuclei had definite atypia. The intra-nodular cell plates or trabeculae were irregular and two or more cells wide, the intra-nodular microvessels were compressed and infiltrated, and there were simultaneously also some dilated blood spaces.

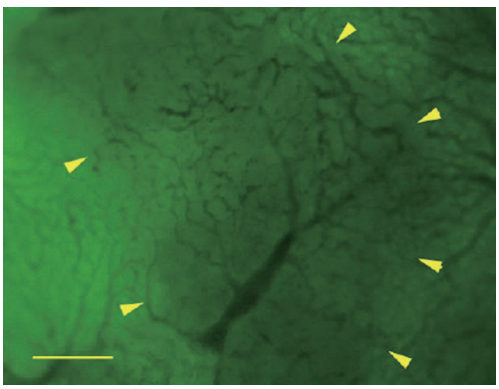

Figure 5 The image of regenerative nodules in cirrhotic liver tissue from an *in vivo* fluorescent microscope. The regenerative nodule (arrow head) is surrounded by cirrhotic liver. The sinusoids appear mildly tortuous and irregular, while they are distributed in a spatially homogeneous fashion (Bar =400 μm).

of five data sets was used as the CD (19).

Statistical analysis

Data were initially assessed for normality with use of normal probability plots and were presented as the mean ± standard deviation. Given the independent and unpaired nature of these data, the Kruskal-Wallis test was initially used to test the overall equality of medians in each data group. When a statistically significant difference was observed, single posttest comparisons of independent samples were performed by using the Mann-Whitney test. An overall difference of $P<0.05$ was considered significant. All statistical analyses were performed with software (SPSS, version 10.0, 1999; SPSS, Chicago, IL, USA).

Results

All rats survived the tumor induction and the *in vivo* microscopy. Ninety hepatic nodules (7 LRNs, 47 DNs, and 36 HCCs) and 45 non-lesion areas (cirrhotic liver) were subjected to *in vivo* microscopy and pathological study.

Morphological and hemodynamic changes of intranodular microvessels evaluated by in vivo fluorescent microscopy

For the background cirrhotic liver and LRN, the sinusoids appeared mildly tortuous and irregular, while they were distributed in a spatially homogeneous fashion. Because the terminal hepatic venules were distributed on the surface of rat liver, the origin of blood flow in sinusoids could not be observed; however, it was observed that the blood flow in sinusoids converged to terminal hepatic venules (*Figure 5*). The size of LRN was 0.87±0.33 cm, and the MVD and BD of regenerative nodules and background cirrhotic liver tissue were 6.38%±1.17% and 35.97±9.41 branches/mm^2 respectively.

For the DN, the intra-nodular microvessels were similar to the sinusoids of background cirrhotic liver tissue, but the diameter and spatial distribution of these microvessels were mildly heterogeneous. The intranodular blood flow passed through the sinusoid-like intra-nodular microvessels and then converged to terminal hepatic venules (*Figure 6*). The nodular size, MVD, and BD of DN were 0.72±0.42 cm, 5.83%±1.83%, and 31.78±13.02 branches/mm^2, respectively.

For the HCC, the intranodular microvessels appeared tortuous, with irregular branching and abrupt diameter changes forming irregularly dilated blood spaces; these convoluted microvessels formed irregular networks in the tumor. The blood flow of the convoluted intra-nodular microvessels drained to the surrounding hepatic sinusoids through the abundant connections between the intratumoral microvessels and the surrounding hepatic sinusoids (*Figure 7*). The nodular size, MVD, BD of HCC were 1.49±0.77 cm, 3.69%±1.51%, and 24.51±7.50 branches/mm^2,

© Quantitative Imaging in Medicine and Surgery. All rights reserved.

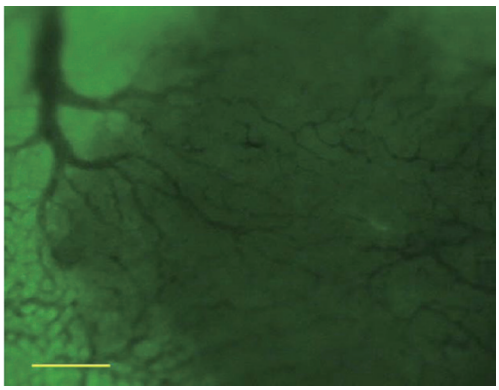

Figure 6 The image of a dysplastic nodule in cirrhotic liver from an *in vivo* fluorescent microscope. The microvessels of dysplastic nodules (the dark area of the image) were similar to the sinusoids of background cirrhotic liver (bottom left corner of the image), but the diameter and spatially distribution of intra-nodular microvessels were heterogeneous compared to the sinusoids of background cirrhotic liver tissue (Bar =400 μm).

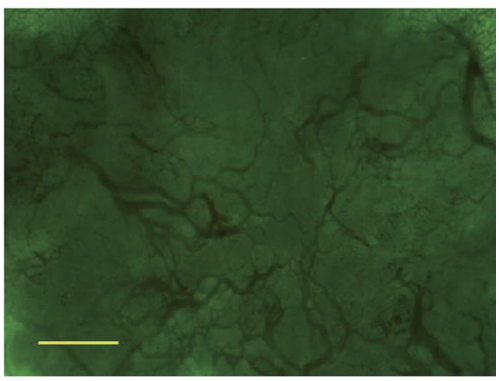

Figure 7 The image of HCC from an *in vivo* fluorescent microscope. The microvessels of HCC appeared tortuous, irregular branching, and abrupt diameter changes to form irregularly dilated blood spaces, these convoluted microvessels constructed irregular networks in the tumor (Bar =1 mm).

respectively.

The MVD and BD of HCCs were less than those of DN and background cirrhotic liver tissue (P<0.05); meanwhile, the BD of DN was also less than that of non-lesion liver parenchyma (P<0.05); however, the MVD of DN was similar to that of non-lesion liver parenchyma (P>0.05) (*Figures 8,9*). The nodular size of HCCs was larger than that of DN and LRNs (P<0.05), but the nodular size of DN was similar to that of LRNs (P>0.05) (*Figure 10*).

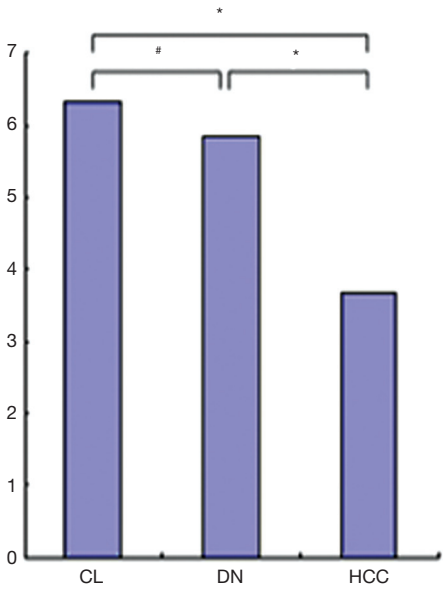

Figure 8 The microvessel density (MVD) of hepatocellular nodules (%). CL, cirrhotic liver; DN, dysplastic nodules; HCC, hepatocellular carcinoma. #P>0.05, *P<0.05.

Histological examination

The CD of HCCs (211.7±17.7 cells per high-power field) was more than that of DN and background cirrhotic liver tissue (130.1±31.1 and 106.3±11.4 cells per high-power field, P<0.05), and the CD of DN was also more than that of background cirrhotic liver tissue (P<0.05) (*Figure 11*).

Discussion

It is widely accepted that accurately distinguishing hepatic nodules with dynamic enhanced CT and MR is very difficult. To resolve this problem, it is important to understand the sequential changes of the intranodular microvessels of these hepatic nodules.

In this study, we analyzed a rat model of chemical hepatocarcinogenesis, which included three consecutive stages: a regenerative nodule, a DN, and HCC. The morphological character of intranodular microvessels was investigated and correlated with histological examination. In concurrence with the progress of hepatocarcinogenesis, the intranodular CD increased, and the intranodular hepatocyte architecture was more irregular; thus, the intranodular MVD decreased, and the irregular convoluted intra-nodular angio-architecture was formed.

For the LRN, there were one or several terminal portal

© Quantitative Imaging in Medicine and Surgery. All rights reserved.

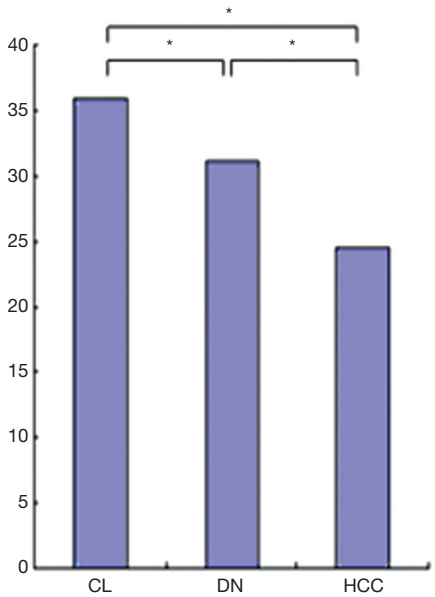

Figure 9 The branch density (BD) of hepatocellular nodules (branches/mm^2). CL, cirrhotic live; DN, dysplastic nodules; HCC, hepatocellular carcinoma. *P<0.05.

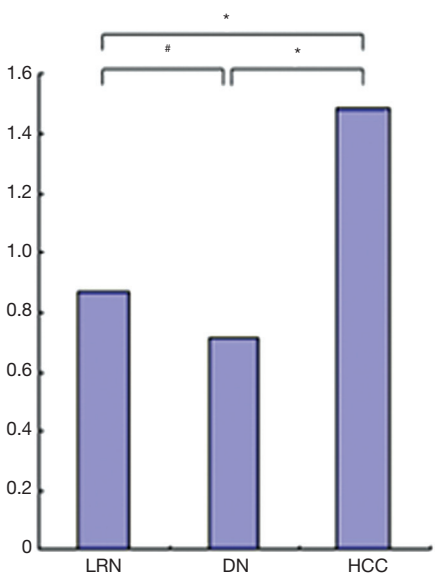

Figure 10 The size of hepatocellular nodules (cm). LRN, large regenerative nodule; DN, dysplastic nodules; HCC, hepatocellular carcinoma. #P>0.05, *P<0.05.

tracts, the hepatocyte plates were one or two cells wide, and the sinusoids were mildly various in diameter. Thus, the intranodular microvessels and blood supply were almost the same as the sinusoids of the background cirrhotic

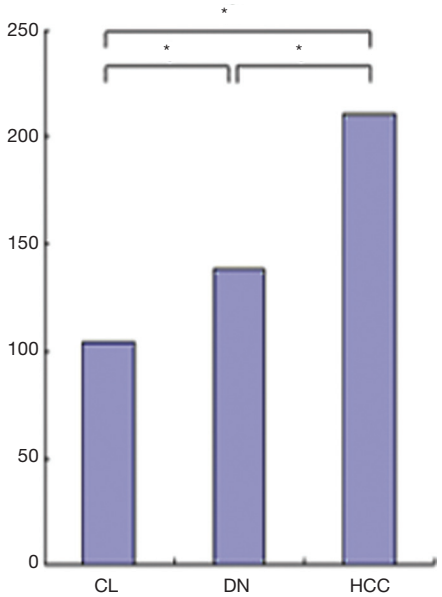

Figure 11 The cell density (CD) of hepatocellular nodules (cells per high-power field). CL, cirrhotic liver; DN, dysplastic nodules; HCC, hepatocellular carcinoma. *P<0.05.

liver tissue, and the LRN could not be distinguished from background cirrhotic liver tissue with enhanced CT and MR (4-7,17,18).

For the DN, the cells of low-grade DNs were usually large and uniform, but there were usually multiple subpopulations of different cellular appearances with various cellular sizes in high-grade DNs. The intra-nodule cell plates were one or several cells wide, and partial intra-nodule sinusoids were compressed, while others were dilated. Thus, the intranodular BD of DN was less than that of non-lesion background cirrhotic liver tissue due to the compression, while the MVD of DN was similar to that of non-lesion background cirrhotic liver tissue due to the dilated intranodule sinusoids. Meanwhile, although the CD of the DNs was a little more than that of background cirrhotic liver tissue, due to the various cell sizes of low- and high-grade DNs, the total volume of the intranodular cell component was similar to that of background cirrhotic liver tissue; that is, the intranodular blood space (MVD) was similar to that of background cirrhotic liver tissue. Because of various blood supplies, the DN could have different enhancement patterns compared to the background cirrhotic liver tissue in the arterial or portal phase of the dynamic enhancement CT and MR images. However, it was isodense or isosignal to the background cirrhotic liver tissue

© Quantitative Imaging in Medicine and Surgery. All rights reserved.

in the parenchyma phase due to the similar MVD of DN and background cirrhotic liver tissue (4-7,17,18).

For the HCCs, the cell size usually decreased, the intranodular cell plates or trabeculae were irregular and two or more cells wide, and the pseudoglandular structure and nontriadal arteries could be found in nodules. The intranodular microvessels were compressed and infiltrated, and there were also some dilated blood spaces in the HCCs. Thus, because of the increased CD and total volume of intranodular cell components in HCCs, the intranodular blood space (MVD and BD) were decreased by the compressing and infiltration of tumor cells. Because of abundant of artery blood supply, HCCs usually appeared distinctly enhanced compared to the background cirrhotic liver tissue in the arterial phase of dynamic enhanced CT and MR images; however, it was hypodense or hyposignal compared to the background cirrhotic liver tissue in the parenchyma phase, which could not be explained simply by artery blood washout due to the homogenous concentration of contrast medium in blood at this time after several recirculations of the contrast medium. This could have resulted from the decreased intranodular MVD and BD of HCC compared to the background cirrhotic liver tissue (1-7,17,18).

In recent years, mounting evidence has suggested that quantitation of intratumor MVD by immunohistochemical staining for endothelial cell markers, such as CD34 and von Willebrand factor (vWF), may be a useful prognostic predictor in cancer patients (20-25), and it has become possible to estimate the histologic grade of malignancy of hepatic nodules through correlation with the imaging of the intranodular blood supply (25-27). However, results of studies on the correlation between the character of enhanced CT or MR imaging of hepatic nodules and immunohistochemical MVD were not homogeneous (20-29). In our opinion, these discrepancies were mainly caused by the complex component of intranodular microvessels, including single proliferated endothelia and newly formed microvessels without lumen, which were CD34 positive, but without blood flow, residual sinusoids, and vasculogenic mimicry, which was itself CD34 negative, but with blood flow (30-32). Meanwhile, the findings presented in this study support the notion that *in vivo* fluorescent microscopy is very similar to contrast enhanced CT or MRI in clinical practice for the evaluation of liver parenchyma micro-circulation. It can be used to explore changes in microcirculation and microvessel architecture in various liver lesions, and it is very important for the further understanding of the changes of the enhancement mode and perfusion parameters of liver lesions in the clinic.

There were several limitations to this study. First, it is well known that chemically induced hepatic nodules, particularly HCCs, vary from well- to poorly differentiated or even undifferentiated in their histologic features. However, our study only focused on well-differentiated HCCs in comparison with other benign hepatocytic nodules and was thus not representative of all possible lesions. Second, the immunohistochemical study should be performed and correlated with the intravital study. In our opinion, the CD34-positive MVD should be well in accordance with the arterial blood supply of hepatic nodules (33-35). However, for intravital observation, it was very difficult to distinguish whether the blood flow of hepatic nodules came from the hepatic artery or portal vein. Third, for the diagnosis and study of hepatic nodules in liver cirrhotic tissue, the four kinds of stepwise-changed hepatic nodules were determined arbitrarily based on the process of the continuous carcinogenesis of hepatic nodules, and this might have had some effect on the results.

Conclusions

In conclusion, in concurrence with the carcinogenesis of the hepatic nodules, the hemodynamic and morphological characteristics of intranodular microvessels varied sequentially with the histological change; namely, the CD increased, and the hepatocyte architecture was more irregular. As a consequence, the intranodular microvessel were compressed and infiltrated, the intra-nodular MVD decreased, and the convoluted microvessels were more irregular. These findings are important for understanding the pathophysiologic and radiological features of hepatic nodules in cirrhotic liver tissue.

Acknowledgments

Funding: This study was sponsored by the National Natural Science Foundation of China (30970810) to Dr. Y Liu. Dr. Y Liu was the principle investigator in this study. The scientific guarantor of this publication is Dr. Y Liu and Dr. PL Li.

Footnote

Conflicts of Interest: The authors have no conflicts of interest to declare.

© Quantitative Imaging in Medicine and Surgery. All rights reserved.

Ethical Statement: This study was approved by the Ethics Review Board of the First Hospital of China Medical University and was performed in accordance with its guidelines.

References

1. Marin D, Di Martino M, Guerrisi A, De Filippis G, Rossi M, Ginanni Corradini S, Masciangelo R, Catalano C, Passariello R. Hepatocellular carcinoma in patients with cirrhosis: qualitative comparison of gadobenate dimeglumine-enhanced MR imaging and multiphasic 64-section CT. Radiology 2009;251:85-95.
2. Kim YK, Kim CS, Han YM, Yu HC, Choi D. Detection of Small Hepatocellular Carcinoma: Intraindividual Comparison of Gadoxetic Acid-Enhanced MRI at 3.0 and 1.5 T. Invest Radiol 2011;46:383-9.
3. Zhao M, Dong L, Liu Z, Yang S, Wu W, Lin J. In vivo fluorescence imaging of hepatocellular carcinoma using a novel GPC3-specific aptamer probe. Quant Imaging Med Surg 2018;8:151-60.
4. International Working Party. Terminology of nodular hepatocellular lesions. Hepatology 1995;22:983-93.
5. International Consensus Group for Hepatocellular Neoplasia. The International Consensus Group for Hepatocellular Neoplasia. Pathologic diagnosis of early hepatocellular carcinoma: a report of the international consensus group for hepatocellular neoplasia. Hepatology 2009;49:658-64.
6. Shinmura R, Matsui O, Kadoya M, Kobayashi S, Terayama N, Sanada J, Demachi H, Gabata T. Detection of hypervascular malignant foci in borderline lesions of hepatocellular carcinoma: comparison of dynamic multi-detector row CT, dynamic MR imaging and superparamagnetic iron oxide-enhanced MR imaging. Eur Radiol 2008;18:1918-24.
7. Shinmura R, Matsui O, Kobayashi S, Terayama N, Sanada J, Ueda K, Gabata T, Kadoya M, Miyayama S. Cirrhotic nodules: association between MR imaging signal intensity and intranodular blood supply. Radiology 2005;237:512-9.
8. Wáng YX, Idée JM. A comprehensive literatures update of clinical researches of superparamagnetic resonance iron oxide nanoparticles for magnetic resonance imaging. Quant Imaging Med Surg 2017;7:88-122.
9. Kan Z, Ivancev K, Lunderquist A, McCuskey PA, Wright KC, Wallace S, McCuskey RS. In vivo microscopy of hepatic tumors in animal models: a dynamic investigation of blood supply to hepatic metastases. Radiology 1993;187:621-6.
10. Gu Y, Scheuer C, Feng D, Menger MD, Laschke MW. Inhibition of angiogenesis: a novel antitumor mechanism of the herbal compound arctigenin. Anticancer Drugs 2013;24:781-91.
11. Schneider G, Seidel R, Uder M, Wagner D, Weinmann HJ, Kramann B. In vivo microscopic evaluation of the microvascular behavior of FITC-labeled macromolecular MR contrast agents in the hamster skinfold chamber. Invest Radiol 2000 35:564-570.
12. Kruskal JB, Thomas P, Kane RA, Goldberg SN. Hepatic perfusion changes in mice livers with developing colorectal cancer metastases. Radiology 2004;231:482-90.
13. Liu Y, Matsui O. Changes of intratumoral microvessels and blood perfusion during establishment of hepatic metastases in mice. Radiology 2007;243:386-95.
14. Weber E, Bannasch P. Dose and time dependence of the cellular phenotype in rat hepatic preneoplasia and neoplasia induced by continuous oral exposure to N-nitrosomorpholine. Carcinogenesis 1994;15:1235-42.
15. Liu Y, Yin T, Feng Y, Cona MM, Huang G, Liu J, Song S, Jiang Y, Xia Q, Swinnen JV, Bormans G, Himmelreich U, Oyen R, Ni Y. Mammalian models of chemically induced primary malignancies exploitable for imaging-based preclinical theragnostic research. Quant Imaging Med Surg 2015;5:708-29.
16. Liu Y, Matsui O. Collaterals through hepatic sinusoids after embolization of terminal portal venules: an in vivo study on mice. Hepatol Res 2005;31:36-42.
17. Kitao A, Zen Y, Matsui O, Gabata T, Nakanuma Y. Hepatocarcinogenesis: multistep changes of drainage vessels at CT during arterial portography and hepatic arteriography--radiologic-pathologic correlation. Radiology 2009;252:605-14.
18. Kim JI, Lee JM, Choi JY, Kim YK, Kim SH, Lee JY, Han JK, Choi BI. The value of gadobenate dimeglumine-enhanced delayed phase MR imaging for characterization of hepatocellular nodules in the cirrhotic liver. Invest Radiol 2008;43:202-210.
19. Vartanian RK, Weidner N. Correlation of intratumoral endothelial cell proliferation with microvessel density (tumor angiogenesis) and tumor cell proliferation in breast carcinoma. Am J Pathol 1994;144:1188-94.
20. Matsubara T, Kanto T, Kuroda S, Yoshio S, Higashitani K, Kakita N, Miyazaki M, Sakakibara M, Hiramatsu N, Kasahara A, Tomimaru Y, Tomokuni A, Nagano H, Hayashi N, Takehara T. TIE2-expressing monocytes as a

© Quantitative Imaging in Medicine and Surgery. All rights reserved.

diagnostic marker for hepatocellular carcinoma correlates with angiogenesis. Hepatology 2013;57:1416-25.
21. Semela D, Dufour JF. Angiogenesis and hepatocellular carcinoma. J Hepatol 2004;41:864-80.
22. Tanigawa N, Lu C, Mitsui T, Miura S. Quantitation of sinusoid-like vessels in hepatocellular carcinoma: its clinical and prognostic significance. Hepatology 1997;26:1216-23.
23. Liu Y, Ye Z, Sun H, Bai R. Grading of uterine cervical cancer by using the ADC difference value and its correlation with microvascular density and vascular endothelial growth factor. Eur Radiol 2013;23:757-65.
24. Möbius C, Demuth C, Aigner T, Wiedmann M, Wittekind C, Mössner J, Hauss J, Witzigmann H. Evaluation of VEGF A expression and microvascular density as prognostic factors in extrahepatic cholangiocarcinoma. Eur J Surg Oncol 2007;33:1025-1029.
25. Park YN, Kim YB, Yang KM, Park C. Increased expression of vascular endothelial growth factor and angiogenesis in the early stage of multistep hepatocarcinogenesis. Arch Pathol Lab Med 2000;124:1061-5.
26. Messerini L, Novelli L, Comin CE. Microvessel density and clinicopathological characteristics in hepatitis C virus and hepatitis B virus related hepatocellular carcinoma. J Clin Pathol 2004;57:867-71.
27. Li Q, Xu B, Fu L, Hao XS. Correlation of four vascular specific growth factors with carcinogenesis and portal vein tumor thrombus formation in human hepatocellular carcinoma. J Exp Clin Cancer Res 2006;25:403-9.
28. Kim YI, Chung JW, Park JH, Kang GH, Lee M, Suh KS, Kim KG. Multiphase contrast-enhanced CT imaging in hepatocellular carcinoma correlation with immunohistochemical angiogenic activities. Acad Radiol 2007;14:1084-91.
29. Wang B, Gao ZQ, Yan X. Correlative study of angiogenesis and dynamic contrast-enhanced magnetic resonance imaging features of hepatocellular carcinoma. Acta Radiol 2005;46:353-8.
30. Pisacane AM, Picciotto F, Risio M. CD31 and CD34 expression as immunohistochemical markers of endothelial transdifferentiation in human cutaneous melanoma. Cell Oncol 2007;29:59-66.
31. Clemente M, Pérez-Alenza MD, Illera JC, Peña L. Histological, immunohistological, and ultrastructural description of vasculogenic mimicry in canine mammary cancer. Vet Pathol 2010;47:265-74.
32. Mihic-Probst D, Ikenberg K, Tinguely M, Schraml P, Behnke S, Seifert B, Civenni G, Sommer L, Moch H, Dummer R. Tumor cell plasticity and angiogenesis in human melanomas. PLoS One 2012;7:e33571.
33. Ruck P, Xiao JC, Kaiserling E. Immunoreactivity of sinusoids in hepatoblastoma: an immunohistochemical study using lectin UEA-1 and antibodies against endothelium-associated antigens, including CD34. Histopathology 1995;26:451-5.
34. Yamamoto T, Kaneda K, Hirohashi K, Kinoshita H, Sakurai M. Sinusoidal capillarization and arterial blood supply continuously proceed with the advance of the stages of hepatocarcinogenesis in the rat. Jpn J Cancer Res 1996;87:442-50.
35. Kim CK, Lim JH, Park CK, Choi D, Lim HK, Lee WJ. Neoangiogenesis and sinusoidal capillarization in hepatocellular carcinoma: correlation between dynamic CT and density of tumor microvessels. Radiology 2005;237:529-34.

Cite this article as: Liu Y, Lu T, Wang C, Li H, Xu K, Li P. Intravital assessment of angioarchitecture in rat hepatocellular nodules using *in vivo* fluorescent microscopy. Quant Imaging Med Surg 2019;9(6):1047-1055. doi: 10.21037/qims.2019.06.11

© Quantitative Imaging in Medicine and Surgery. All rights reserved.